Modelling the Effect of Bow Profile Variations on Naval Ship for Optimizing Resistance Using Computational Fluid Dynamics

Bagiyo Suwasono[1], Supartono[1], Sutiyo[1], Ali Munazid[1], Karyawan[2], Feronika Sekar Purininingsih[2]

This study closely examines the intricate relationship between bow profiles and the hydrodynamic resistance experienced by naval vessels, employing Computational Fluid Dynamics (CFD) as a pivotal tool for analysis. The study examined three distinct bow configurations: no-axe, semi-axe, and fully-axe designs. The primary objective of this study was to ascertain which of these configurations most effectively minimizes hydrodynamics resistance, which is a critical factor in enhancing the performance and efficiency of naval ships. Through a series of detailed CFD simulations, the finding revealed that both the semi-axe and fully-axe designs significantly reduced resistance compared to the traditional no-axe bow design. The semi-axe design achieved an impressive average reduction of 9.17%, whereas the fully-axe configuration followed closely with a reduction of 7.64%. Interestingly, the semi-axe bow surpasses the fully-axe design in terms of resistance reduction and provided an additional advantage of 1.42%, underscoring its superior hydrodynamics performance compared to the fully-axe design. These results underscore the potential benefits of adopting innovative bow shapes in naval architecture, particularly regarding operational efficiency. The simulations further indicated that the alternative bow design contributed to a notable decrease in the wave height during the vessel's interaction with water. By refining bow shapes, naval forces can enhance not only the speed and agility of their vessels but also their overall mission effectiveness, particularly in challenging maritime environments. The implications of this research extend beyond more performance metrics; they highlight the critical need for ongoing innovation in vessel design to meet the evolving challenges of maritime security and operational readiness.

KEYWORDS
~ Navy ship
~ CFD
~ Resistance
~ Bow variations

[1] Universitas Hang Tuah, Surabaya, Indonesia
[2] National Research and Innovation Agency, Tangerang Selatan, Banten, Indonesia
e-mail: bagiyo.suwasono@hangtuah.ac.id
doi: 10.7225/toms.v15.n01.006

Received: 15 Oct 2024 / Revised: 10 Sep 2025 / Accepted: 29 Dec 2025 / Published: 20 Apr 2026

1. INTRODUCTION

Indonesia is the world's largest archipelagic state, consisting of over 17,000 to 18,000 islands stretching approximately 5,200 km along the equator (Cribb & Ford, 2009). This vast collection of islands, located between the Indian and the Pacific Oceans, ranges from Sabang to Merauke and forms a unique cluster that is considered a single entity under the concept of an archipelagic country. Two-thirds of Indonesia's area is covered by the sea, which connects 17,504 islands and emphasizes its maritime nature (Djunarsjah and Putra, 2021). As an archipelagic state, Indonesia exercises sovereignty not only over its land territory but also over the waters between the islands, highlighting the integral role of both land and sea in its national identity (Butcher & Elson, 2017).

Indonesia's unique status as an archipelagic state presents a range of opportunities and challenges that must be addressed carefully. Proactive initiatives aimed at addressing the impacts of climate change are crucial as environmental factors can exacerbate these vulnerabilities. By capitalizing on its strategic geographical position and leveraging diplomatic relationships, Indonesia has the potential to significantly bolster maritime security (Priestnall, 1997). A comprehensive strategy is essential for effectively addressing these security concerns. This strategy should encompass legal reforms to update and strengthen existing laws, reorganization of institutions to improve efficiency and responsiveness, and fostering enhanced cooperation with regional partners (Febrica, 2017). To address these challenges, Indonesia requires a strong naval fleet and improved governance. The government has identified enhanced connectivity as crucial for promoting economic growth, especially in the manufacturing sector (Sandee, 2016). Establishing a mechanism for cross-institutional coordination could lead to more effective marine protection and security measures in Indonesia (Sahri *et al*., 2020). Additionally, this enhancement of security measures is vital for safeguarding the nation's sovereignty against evolving threats, including piracy, illegal fishing, and territorial disputes (Darmawan, 2022). Through a concerted effort that combines legal, institutional, and cooperative frameworks, Indonesia can address immediate security challenges and position itself as a resilient player in the regional and global maritime landscapes (Lau, 2024).

Naval ships are designed to operate optimally at high speeds, and research on high-speed naval ships, particularly the bow sections, continues to evolve to improve their performance and efficiencies. *Keuning et al*., (2015) explored the feasibility of applying an axe bow to a 5,000-ton frigate, highlighting its benefits in reducing resistance and enhancing seakeeping capabilities. Research indicates that vessels operating at Froude numbers (Fr) between 0.4 and 0.5 exhibit improved hydrodynamic characteristics when specific design modifications are implemented. A novel bow appendage can reduce the total resistance by more than 8% at optimal effectiveness (Liu *et al*., 2020). Similarly, Kusuma *et al*., (2020) demonstrated that redesigning the KCR 60m-class fast missile boat with an axe bow resulted in a 2.75% to 11.5% reduction in resistance, improving fuel efficiency and speed. An axe bow installed on the main hull of the trimaran model can reduce the amount of drag experienced by the vessel by up to 8% (Utama *et al*., 2021). Additionally, Kiryanto *et al*., (2021) examined the impact of adding an anti-slamming bulbous bow to tugging supply vessels, revealing significant reductions in total resistance through computational fluid dynamics (CFD) simulations. These studies underscore the ongoing advancements in naval architecture aimed at improving the efficiency and performance of vessels.

Rijkens and Mikelic, (2022) further validated these findings through hydrodynamic comparisons, showing superior drag reduction and wave-cutting ability for axe bow hulls compared to conventional designs. Recent studies have explored various aspects of hull design and their influence on ship resistance, particularly focusing on innovative bow configurations. Samuel *et al*. (2023) conducted a numerical study on the Ulstein X-Bow configuration and analyzed the impact of water depth on the total resistance, which is critical for optimizing vessel performance under varying operational conditions. In another study, Samuel *et al*. (2023) investigated the effects of an inverted bow on frigate-hull resistance, highlighting its potential to reduce drag and improve hydrodynamic efficiency. Similarly, Fitriadhy *et al*. (2023)performed computational analyses on axe bow ships, demonstrating the importance of predicting total resistance in calm water to enhance design accuracy and operational effectiveness. Finally, Suardi *et al*. (2023) emphasized the positive impact of axe bows on patrol ships, noting improvements in resistance, freeboard, and trim, which enhance stability and operational effectiveness in rough seas. Together, these studies underscore the versatility and advantages of axe-bow technology for modern naval vessels.

Although there are currently no widespread examples of axe bow-equipped naval ships in service, ongoing research and experimental data underscore their potential for adoption in various naval platforms. As navies continue to prioritize advanced technologies for superior maritime capabilities, the axe bow design is likely to gain further traction in future fleet developments, and variations in the combinations of conventional and axe bow (semi-axe bow) designs are worth exploring.

This study evaluated the performance of naval ships with three bow variations: no-axe, semi-axe, and fully-axe bows, focusing on minimizing resistance. A Computational Fluid Dynamics (CFD) approach was employed to analyze the hydrodynamic effects of these bow designs on ship resistance. The CFD procedure included a rigorous verification process for the simulations to ensure the accuracy and reliability of the obtained results. This verification step involved validating the numerical models against benchmark data and refining the mesh resolutions, time step settings, and turbulence models to

achieve convergence. By simulating various operational conditions, this study aimed to quantify the impact of each bow design on wave-making resistance, pressure distribution, and flow patterns.

2. MATERIAL AND METHODS

2.1. Governing Equation

Computational Fluid Dynamics (CFD) was used to predict the resistance of the models. Utama *et al*. (2021) conducted research on calculating the hull resistance of a trimaran model with axe bow modification using CFD showed good results compared to experiments. The CFD model employed a three-dimensional equation using the Reynolds-averaged Navier-Stokes (RANS) technique. The flow problems in the walls of a ship were solved using a steady incompressible flow, as provided by ANSYS (2020).

The selection of turbulence models is important for modelling wake fields. In this study, the Shear Stress Transport (SST) turbulence model was developed by Menter (1993, 1994). The SST model has been utilized and verified by many researchers, all of whom have reported positive findings using the model (Menter *et al*., 2003). A RANS solver implemented in ANSYS CFX was used to solve the fluid flow fields. Equations (1), (2), and (3) illustrate the continuity, RANS, and SST turbulence equations, respectively.

Continuity equation:

$$\frac{\partial \rho}{\partial t} + \frac{\partial}{\partial x_j}\left(\rho U_j\right) = 0 \qquad (1)$$

where ρ is the fluid density, *t* is the time, *and* U_j is the flow velocity vector.

RANS equation:

$$\rho \bar{f}_i + \frac{\partial}{\partial x_j}\left[-\bar{p}\delta_{ij} + \mu\left(\frac{\partial \bar{u}_i}{\partial x_j} + \frac{\partial \bar{u}_j}{\partial x_i}\right) - \overline{\rho u_i' u_j'}\right] - \rho \bar{u}_j \frac{\partial \bar{u}_i}{\partial x_j} = 0 \qquad (2)$$

The mean momentum of a fluid element owing to mean flow unsteadiness is shown on the left-hand side of the RANS equation. That modification is compensated the mean body force ($\bar{f}$), the mean pressure field ($\bar{p}$), the viscous stress, $\mu\left(\frac{\partial \bar{u}_i}{\partial x_j} + \frac{\partial \bar{u}_j}{\partial x_i}\right)$, and apparent stress ($\rho u_i' u_j'$) to the fluctuating velocity field.

Menter's SST equation:

$$\frac{\gamma}{v_t} P - \beta \rho \omega^2 + \frac{\partial}{\partial x_j}\left[\left(\mu + \sigma_\omega \mu_t\right)\frac{\partial \omega}{\partial x_j}\right] + 2(1 - F_1)2\rho_{\omega 2}\frac{1}{\omega}\frac{\partial k}{\partial x_j}\frac{\partial \omega}{\partial x_j} - \left(\frac{\partial(\rho\omega)}{\partial t} + \frac{\partial(\rho u_j \omega)}{\partial x_j}\right) = 0 \qquad (3)$$

Menter's SST model combines the benefits of the k–ω and k–ε turbulence models to produce an effective model formulation for a broad range of applications. To accomplish this, a blending function F1 is added, which is equal to one in the region close to the solid surface and zero in the flow domain far from the wall. Specifically, it triggers the k–ε model for the residual flow and k–ω wall area. This method allows the free-stream sensitivity to benefit from the promising near-wall performance of the k–ω model.

2.2. Geometry Model

The modelling process was performed on conventional, axe, and semi-axe bow ships. The semi-axe bow serves as a transitional form between the no-axe and axe bows. For consistency in terminology, the conventional bow shape is referred to as a no-axe bow, and the axe bow is referred to as a fully-axe bow. Consequently, the different bow shapes were categorized as no-axe, semi-axe, and fully-axe bows, as shown in Figure 1. The main dimensions of the model are presented in Table 1.

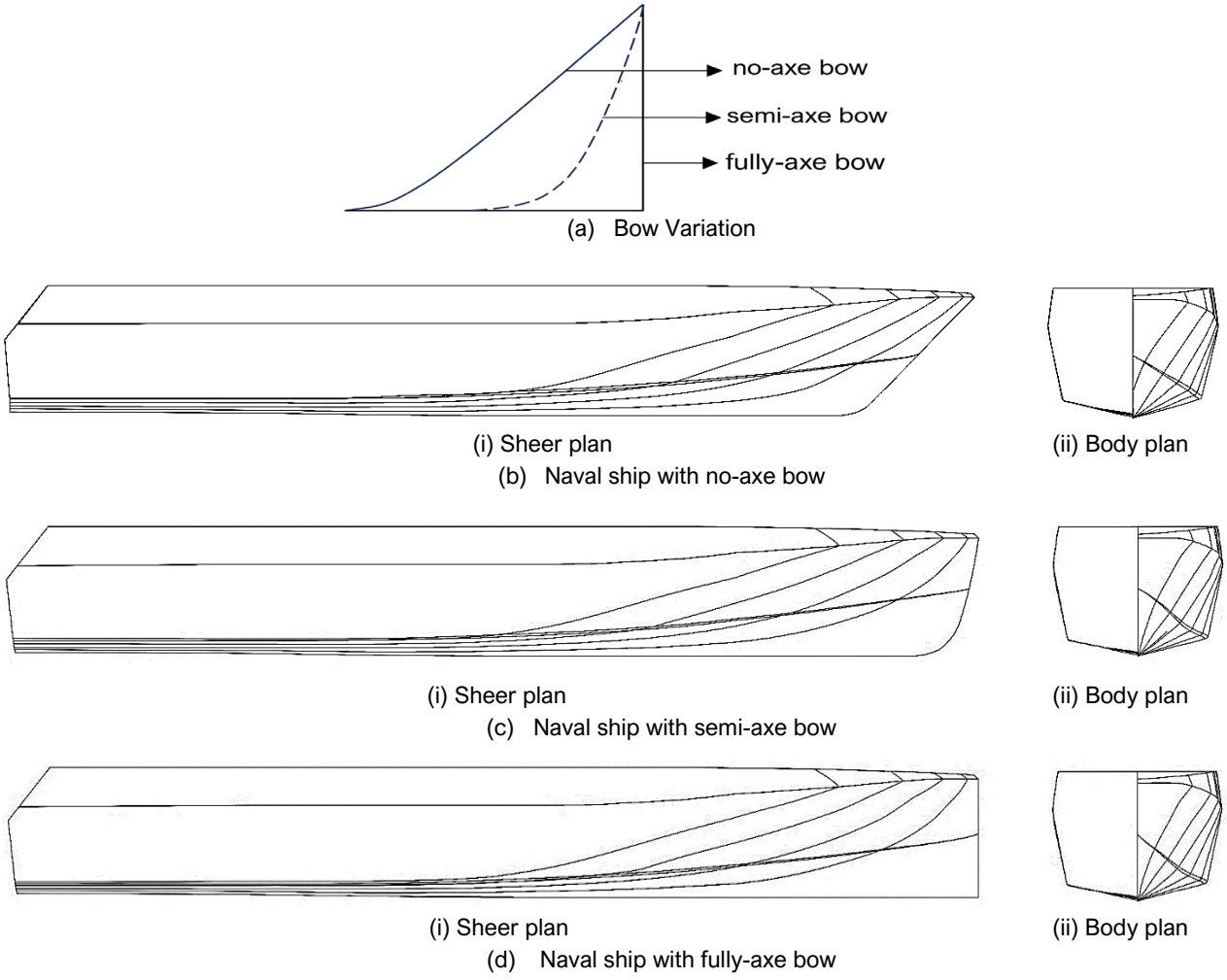

Figure 1. Lines plan of naval ship with bow profile variations

Dimension	Unit	No-Axe Bow	Semi-Axe Bow	Fully-Axe Bow
Length over All (L_{oA})	m	2	2	2
Length Water Line (L_{WL})	m	1.823	1.949	2
Breadth (B)	m	0.356	0.356	0.356
Height (H)	m	0.265	0.265	0.265
Draught (T)	m	0.69	0.69	0.69
Wetted Surface Area (WSA)	m	0.566	0.57	0.578
Displacement (Δ)	kg	20.84	20.98	20.98
Coefficient Block (C_B)	-	0.534	0.5	0.49

Table 1. Main dimensions of naval ship model

2.3. Boundary Setting

The computational domain that was suggested most for the velocity inlet was set at 2 L ahead perpendicular to the front, and the domain that was recommended for the outlet pressure was set at 5 L towards the rear, which was determined perpendicular to the front. It was decided that setting the transverse and vertical directions to 2L-3L would prevent the side borders from being affected by backward flow (Nasirudin *et al*. 2025).

The boundary conditions and domain dimensions are shown in Figure 2. The following opening condition was applied to the top wall, and a symmetry condition was applied to the side walls. The hull body was defined as a fixed boundary, and a no-slip condition was imposed on the model. At the inlet, the flow rate was set to Fr = 0.3 – 0.7, and the pressure at the outlet was set as a function of the water level. Specifying the volume fraction functions of water and air at

the entry and exit points of the system is another method for describing the initial free surface location. This function was used to determine the amounts of water and air present in the system.

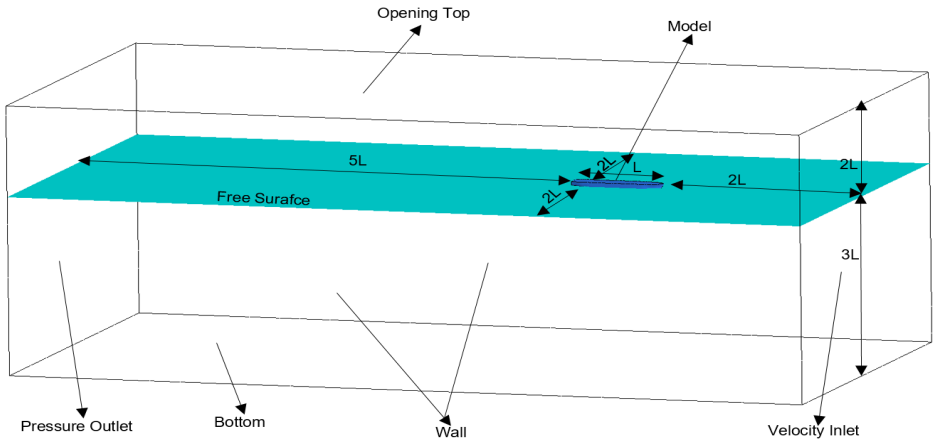

Figure 2. Boundary conditions of model

2.4. Grid Independence Study

A Design modeller was used to perform the mesh generation. The combination of structured and unstructured meshes used to discretize the computational domain is referred to as a hybrid mesh (HM). Considering the intricate geometrical features of the hull, a mesh with triangular elements was constructed on the hull surface, and the boundary layer was refined with prism elements by expanding the surface-mesh node. As shown in Figure 3, the tetrahedral elements were inflated to cover the area, whereas in the distant field, an unstructured mesh with grid generation was formed to reduce the number of elements.

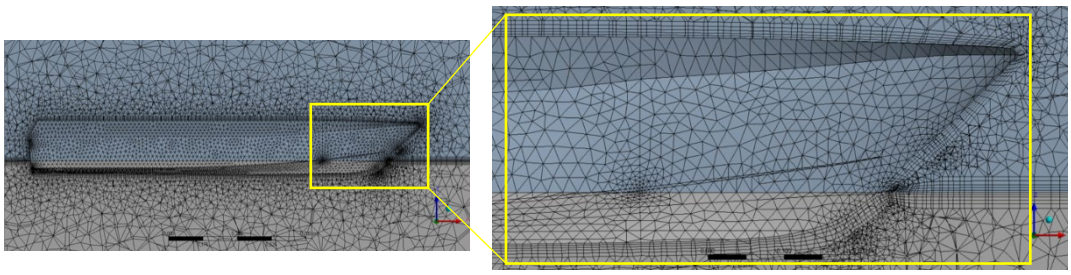

(a) Naval ship

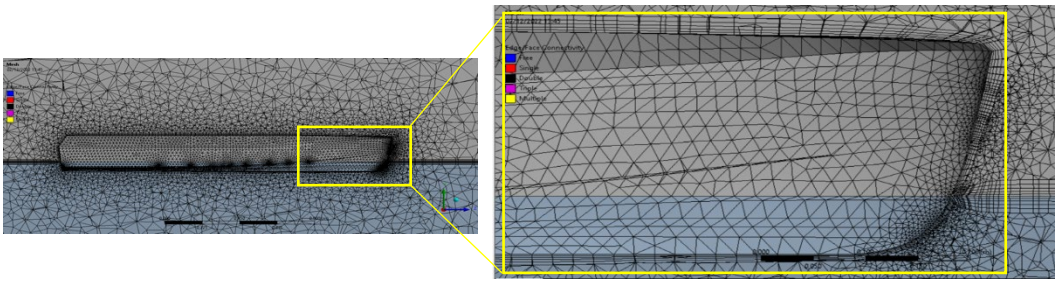

(b) Naval ship with semi-axe bow

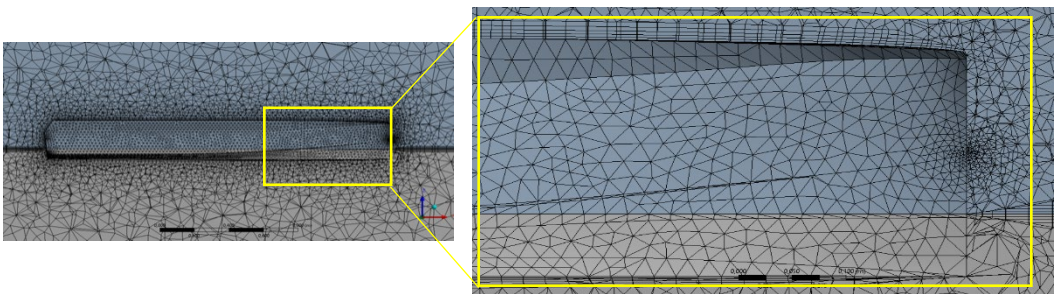

(c) Naval ship with fully-axe bow

Figure 3. Hybrid mesh of naval ship model

A fine mesh may always deliver reliable results in ANSYS CFX; however, at the same time, it increases the computational cost and time consumption owing to the large number of elements. The mesh size plays a significant role in the calculations. Mesh convergence experiments were performed for the Navy ship models at a Froude number of 0.3 to establish the mesh size that would provide an acceptable level of numerical accuracy and total number of elements. The grid independence study is shown in Figure 4, where the number of elements used is approximately 1.7M. It is evident that the use of CFD makes a significant contribution to naval ship model simulations. These results were verified using a grid-independence study with disparities of less than 2% (Anderson, 1995).

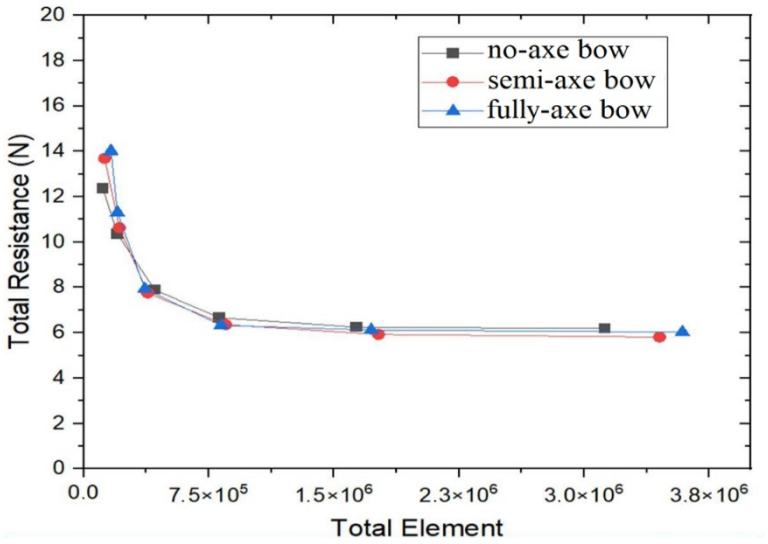

Figure 4. Grid independence study of naval ship model

2.5. Grid Uncertainty Analysis

ITTC (2017) suggested that uncertainty analysis is the foundation of grid convergence studies. Convergence analysis was conducted using three different mesh resolutions, which were subsequently categorized as coarse, fine, and the finest. The mesh was altered by adjusting the size of the individual faces while maintaining the overall size of the object constant by using a uniform element size. This was performed to achieve this goal. Because the mesh resolution was defined by the standard wall calculation, the inflation layer was consistently maintained throughout the investigation, as shown in Table 2.

Furthermore, this approach can be extended to investigate additional parameters. The refinement ratio is recommended to have a value of $\sqrt{2}$, given that it is sufficiently high to allow for sensitivity to changes in the parameters and sufficiently low to enable the generation of at least three subsequent solutions while maintaining stability. Although a minimum required mesh size of three is specified, it is permissible to use a higher refinement ratio if inclined.

Oscillatory convergence is a phenomenon observed in numerical simulations in which the solution exhibits oscillatory behavior as the resolution of the computational grid increases. This behavior typically emerges during a three-stage grid refinement process, leading to oscillations that can compromise the accuracy and stability of the computed solution. The relationship governing this behavior is encapsulated in the R value, which is defined by the equation

$$R = \frac{f_1 - f_2}{f_2 - f_3} \qquad (4)$$

where f_1, f_2, f_3, f_4 The calculation result and the interpretation of the R value is critical for understanding the nature of convergence: when 0<R<1, the convergence is classified as monotonic; for R<0 and |R|<1, it is identified as oscillatory convergence; R>1 indicates monotonic divergence; and for R<0 with |R|>1, the divergence is categorized as oscillatory. This framework is essential for analyzing the performance of numerical methods in computational simulations.

The outcomes, which are presented in Table 3, were computed using the formulas specified in the section on utilized equations.

Model	Detail	Coarse (1)	Fine (2)	Finest (3)
No-Axe Bow	Body sizing (m)	0.25	0.20	0.15
	Face sizing (m)	0.02	0.015	0.01
	Number of elements (NE)	812,466	1,635,860	3,124,883
	Total resistance (R_T)(N)	6.67	6.25	6.19
Semi-Axe Bow	Body sizing (m)	0.25	0.20	0.15
	Face sizing (m)	0.02	0.015	0.01
	Number of elements (NE)	851,245	1,768,692	3,452,681
	Total resistance (R_T)(N)	6.36	5.93	5.81
Fully-Axe Bow	Body sizing (m)	0.25	0.20	0.15
	Face sizing (m)	0.02	0.015	0.01
	Number of elements (NE)	823,665	1,723,365	3,589,978
	Total resistance (R_T)(N)	6.33	6.12	6.04

Table 2. Three varying mesh resolution details of naval ship models

Outcome	Equation	No-Axe Bow	Semi-Axe Bow	Fully-Axe Bow
Difference of estimation	$\varepsilon_{21}=NE_2/NE_1$	2.0135	2.0778	2.0923
	$\varepsilon_{32}= NE_3/NE_2$	1.9102	1.9521	2.0831
Refinement ratio	$r_{21}=R_{T2} -R_{T1}$	-0.4200	-0.4303	-0.2052
	$r_{32} = R_{T3} -R_{T2}$	-0.0600	-0.1172	-0.0898
Convergence	$R_i=\varepsilon_{32}/\varepsilon_{21}$	0.1429	0.2725	0.4375
Order of accuracy	$p=\ln(\varepsilon_{21}/\varepsilon_{32})/\ln(r_i)$	-2.7805	-1.7780	-1.1198
Extrapolated relative error	$e_{21}= \varepsilon_{21}/r_i^p-1$	-0.1375	-0.1297	-0.0608
	$e_{32}= \varepsilon_{32}/r_i^p-1$	-0.0226	-0.0417	-0.0269
Grid convergence index (GCI)	$GCI_{21}=Fs\|e_{21}\|$	0.5880	0.3329	0.0957
	$GCI_{32}= Fs\|e_{32}\|$	0.0733	0.0828	0.0423

Table 3. The uncertainty analysis performed for naval ship models

The analysis of grid convergence for the naval vessel is presented in Table 3, which presents a detailed evaluation of the Grid Convergence Index (GCI) and oscillation convergence metrics. The simulation results indicated a commendable level of precision, with GCI_{21} values recorded between 0.0957% and 0.5880%, and GC_{32} values ranging from 0.0423% to 0.0733%. Both GCI values were significantly below the established threshold of 5%, reflecting a favourable outcome in the convergence assessment. The low percentages observed in the GCI metrics suggest that the parameters under investigation operate effectively within the acceptable limits defined in this study. This finding is crucial because it underscores the reliability of the simulation results, indicating that the grid resolution is sufficient to capture essential physical phenomena without introducing significant numerical errors.

The analysis conducted in this study went beyond a mere evaluation of the Global Convergence Index (GCI) to encompass a more comprehensive assessment through the calculation of oscillatory convergence, denoted as Ri. The results of this calculation yielded values ranging from 0.1429 to 0.4375. This specific range of Ri values is particularly significant because it indicates the state of monotonic convergence. In mathematical terms, monotonic convergence occurs when a sequence consistently approaches its limit without oscillating or diverging. The fact that the Ri values fall within the interval of 0 and 1 ($0 < Ri < 1$) further reinforces this observation. The implications of these findings are thus significant. The observed Ri values suggest that the simulation process employed in this analysis demonstrated both stability and high reliability. In this context, stability refers to the ability of the numerical method to produce consistent results over time, whereas reliability indicates that the method can be trusted to accurately reflect the underlying dynamics of the studied system. In this case, the system in question pertains to the dynamic behaviour of naval vessels.

The SST k-ω model incorporates Automatic Wall Treatment to effectively manage high y+ regions, specifically those where the y+ value ranges from 30 to 300. In these areas, logarithmic wall functions were employed to approximate the turbulence behaviour near the wall. Furthermore, maintaining a y+ value below 300 (Figure 5) enhances the computational efficiency by allowing the use of coarser mesh configurations in noncritical regions. This approach significantly decreased the total number of cells required, thereby facilitating faster simulations.

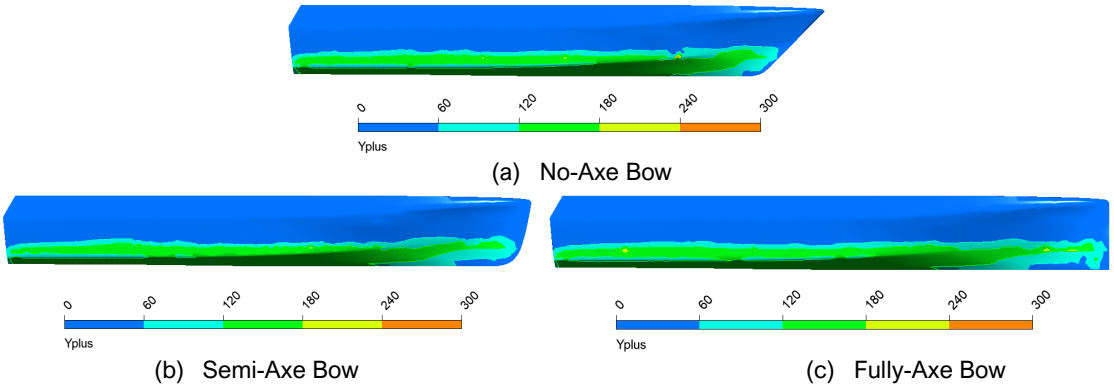

(a) No-Axe Bow

(b) Semi-Axe Bow

(c) Fully-Axe Bow

Figure 5 y^+ value for variation models

The SST k-ω turbulence model offers significant benefits in situations where there is a need to strike a balance between computational efficiency and accuracy, making it especially useful in applications such as ship resistance analysis and other marine engineering tasks. In scenarios characterized by high y+ values, specifically within the range of 30 – 300, the model utilizes logarithmic wall functions to effectively approximate the behavior of turbulence near the wall surfaces (ANSYS, 2020). This methodology facilitates the implementation of coarser mesh configurations near the walls, thereby leading to a substantial decrease in computational expenses while ensuring that the accuracy of the results remains acceptable (Krank, 2019).

3. RESULTS AND DISCUSSION

3.1. Total Resistance and Correlation with Block Coefficient

The resistance calculations for a naval ship with no-axe, semi-axe, and fully-axe bow modifications were presented and compared in this study. The positive results from the CFD resistance estimates are shown in Figure 6, owing to the utilization of the semi-axe and fully-axe bows. CFD analyses revealed an estimated drag reduction of up to 11.18% when using a semi-axe bow hull with a lower value than that of the no-axe bow hull. Similarly, the fully-axe bow hull exhibited less resistance than the no-axe bow hull, with a decrease of up to 10.00%. As previously stated, Bouckaert (2012) demonstrated that an axe bow can reduce drag by up to 10% compared with a no-axe bow profile, and Utama *et al*. (2021) found similar results for monohull ships using fully-axe bow. The development of the semi-axe bow had a positive impact, as its use reduced the resistance by an average of 1.42% compared to the use of a no-axe bow profile hull. The simulation results indicate that the axe-bow design significantly reduces resistance, achieving a reduction of up to 9% for frigate vessels (Keuning *et al*., 2015, 2018; Rijkens & Mikelic, 2022) .

There is a direct correlation between the block coefficient and hull shape factor of a naval ship. The no-axe and semi-axe bow naval ships had CB values of 0.534 and 0.50, respectively. A semi-axe bow navy ship has a CB value that is 6% lower than that of a no-axe bow naval ship, which results in an average reduction contribution of 8%. In addition, fully-axe bow naval ship has a CB value of 0.49, which is 8% lower than the CB value of a no-axe bow naval ship. A total resistance reduction of approximately 7% was achieved by the fully-axe bow naval ship. A lower value is associated with this reduction compared to that of a naval ship with a semi-axe bow. This phenomenon could be influenced by the fact that the wetted surface area of a naval ship with a semi-axe bow is less than that of a naval ship with a fully-axe bow.

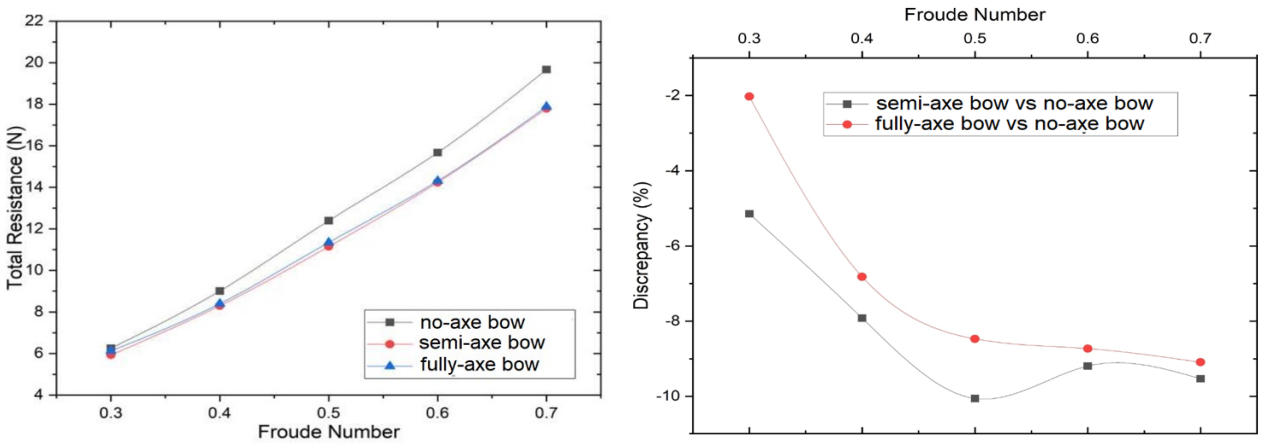

(a) Total resistance (b) Discrepancy

Figure 6. CFD simulation result of total resistance and its discrepancy at Navy ship

3.2. Resistance Component

The CFD simulation is described in Section 3.1, where the total resistance was calculated. ANSYS software can decompose the total resistance into two distinct components: viscous and pressure resistance. Viscous resistance refers to the frictional forces that arise due to the viscosity of the fluid as it flows over surfaces, whereas pressure resistance is defined as the resistance encountered by the fluid as it moves through a medium, which is often associated with wave dynamics. This separation of resistance types allows for a more nuanced understanding of fluid behaviour in various applications, enabling engineers and researchers to optimise designs and improve performance by addressing each resistance component. This formula was used to calculate the viscous and wave resistances. The total resistance is the sum of the viscous and wave resistances, as formulated in Equation 5, and William Froude was the first researcher to introduce the description of total resistance into several components. The total resistance is the sum of the two types of resistances.

$$R_T = R_V + R_W \tag{5}$$

where R_T represents the overall resistance measured in N, while R_V denotes the resistance attributed to viscous, also expressed in N. Additionally, R_W refers to the wave resistance, which is similarly quantified in N.

The wave resistance trends reveal a nonlinear relationship with speed across various designs, characterized by a gradual increase at lower velocities that becomes more pronounced as the speed increases, as shown in Figure 7. Among the different bow designs, the fully axe bow consistently exhibited the lowest wave resistance, particularly at speeds of approximately 2.4 m/s. In contrast, the no-axe bow demonstrated the highest wave resistance across all tested speeds, making it the least efficient option. The semi-axe bow occupies a middle ground, providing a moderate enhancement in wave resistance compared to the no-axe design, thus offering a balanced performance for those seeking a compromise between efficiency and speed.

Figure 7 explains that viscous resistance tends to increase with speed although this increase follows a more linear pattern than wave resistance. In terms of bow design, the variations in performance were relatively minor; however, the fully-axe bow generally exhibited a slight advantage in terms of lower resistance at higher velocities. This observation indicates that the viscous drag is less influenced by the shape of the bow than the wave-making drag, suggesting that the design of the bow plays a more significant role in the latter type of resistance. Consequently, while optimizing for speed, attention to bow shape may yield diminishing returns in terms of viscous resistance, emphasizing the need to focus on wave-making characteristics to enhance performance.

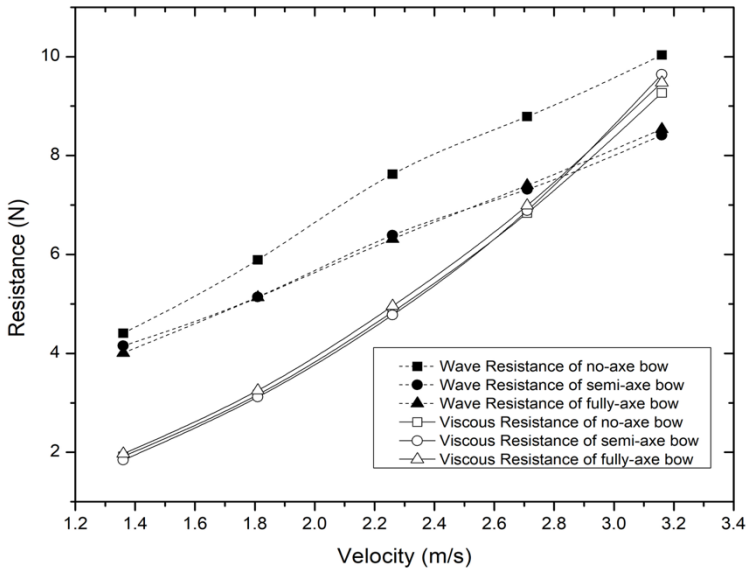

Figure 7 Resistance component of naval ship model

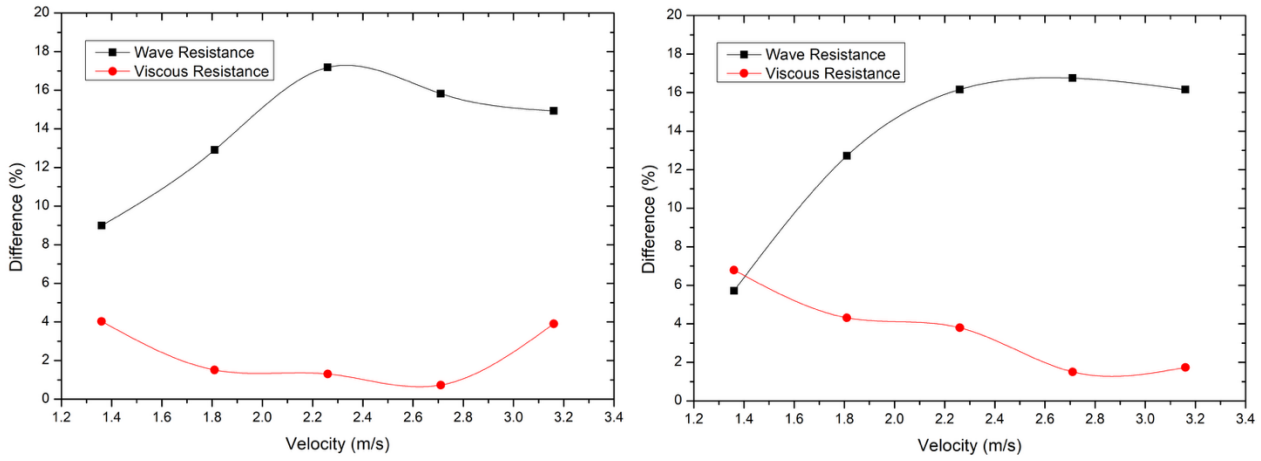

(a) The difference in resistance components between no-axe bow and semi-axe bow naval ships

(b) The difference in resistance components between no-axe bow and fully-axe bow naval ships

Figure 8 Difference in resistance components between naval ships

The analysis of wave resistance, represented by black squares (Figure 8(a)), indicates that the semi-axe bow begins with a reduction of approximately 6% at a speed of 1.4 m/s. As the speed increased, this reduction steadily increased, reaching a peak of approximately 13 - 14% lower at approximately 2.4 m/s. Following this peak, the wave resistance gradually diminished, settling at approximately 10% lower when the speed reached 3.2 m/s. Overall, the average reduction in wave resistance across the entire speed range was estimated to be between 11% and 12%, highlighting the semi-axe bow's effectiveness in enhancing hydrodynamic efficiency primarily through its impact on wave-making resistance.

Furthermore, the viscous resistance, denoted by red circles (Figure 8(a)), remained relatively low and stable throughout the tested speed range, showing only minor fluctuations between 1% and 3% lower for the semi-axe bow. The average reduction in viscous resistance was approximately 2%, suggesting that the modifications to the bow shape had a limited effect on the skin friction drag. The most significant advantages in wave resistance were observed at approximately 2.4 m/s, where the effects of wave-making were most pronounced, underscoring the importance of bow design in optimising performance under specific speed conditions.

The examination of wave resistance, depicted by the black curve (Figure 8(b)), reveals that at a speed of 1.4 m/s, the fully axe bow achieves a notable reduction of approximately 6% in wave resistance. As the speed increases to approximately 2.4 m/s, this reduction escalates to its maximum, demonstrating a significant decrease of approximately 17-18%. However, as the speed further increased to 3.2 m/s, the wave resistance experienced a slight decline, resulting in a reduction of approximately 14%. When averaging the results across all tested speeds, the fully axe bow consistently showed

a reduction in wave resistance estimated to be approximately 13 - 14%. This considerable decrease is instrumental in improving the overall efficiency of the vessel, highlighting the importance of bow design in the hydrodynamic performance.

In contrast, the analysis of viscous resistance, represented by the red curve (Figure 8(b)), starts with a similar reduction of approximately 6% at 1.4 m/s but gradually diminishes as the speed increases, ultimately resulting in a reduction of only 1 - 2% at 3.2 m/s. The average reduction in viscous resistance for the fully axe bow was relatively modest, estimated at approximately 3 - 4%. This indicates that the bow shape has a lower influence on the hull surface area and wetted geometry than the pronounced effects of wave-making. Notably, the most significant efficiency improvements were observed at approximately 2.4 m/s, where the impact of wave formation was most pronounced, thereby underscoring the critical role of bow design in optimising hydrodynamic efficiency.

Figure 9 shows that the bow part of the ship also affects the fluid interaction with the hull, with the axe bow causing fluid interactions that create fewer waves in the forward region of the bow than those of the other bows. The CFD analysis demonstrated that the no-axe bow hull generated more waves than the axe-bow hull did. Therefore, the resistance provided by the hull depends on whether it has an axe bow. The no-axe bow naval ship provides more resistance than the hulls with semi-axe and fully-axe bows.

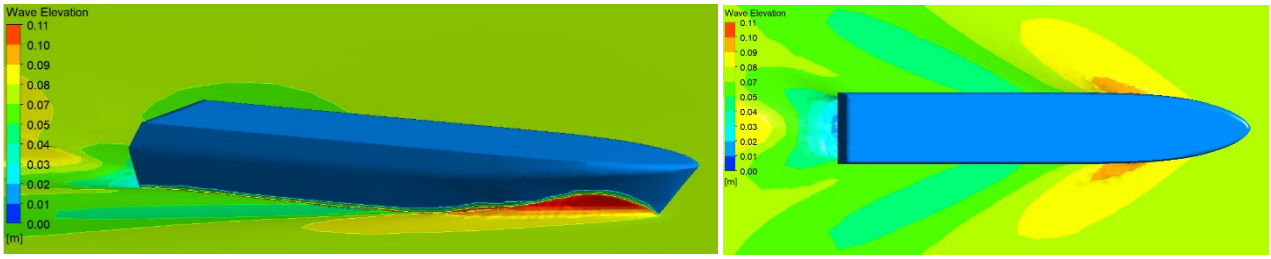

(a) Naval ship with no-axe bow

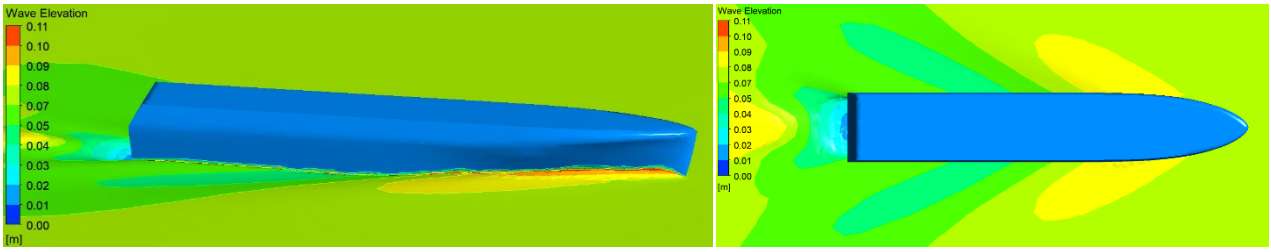

(b) Naval ship with semi-axe bow

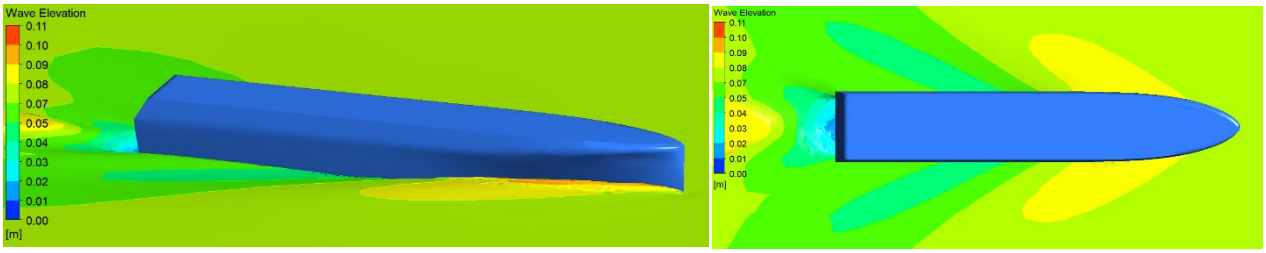

(c) Naval ship with fully-axe bow

Figure 9. Wave elevation at Fr=0.7

Furthermore, the fluid interaction with the hull is affected by the bow of the navy ship. Fluid interaction tends to produce higher waves in the bow section of the no-axe bow naval ship, as shown in Figure 9(a). The CFD simulation clearly shows that the bow section with the hull modified with a semi-axe bow produces less wave-making than the no-axe bow, as shown in Figure 9(b). As shown in Figure 9(c), the effect of the axe bow modification on the bow of the naval ship resulted in low wave-making. This affects the resulting resistance so that the hull with a modified bow shape with a semi-axe and fully axe bows have less resistance than the hull with no-axe bow.

4. CONCLUSION

This study utilized Computational Fluid Dynamics (CFD) to evaluate the hydrodynamic resistance of naval ships with different bow profiles: no-axe, semi-axe, and fully-axe designs. The primary aim of this study was to identify the configuration that minimizes hydrodynamic resistance, thereby enhancing naval vessel performance and efficiency. The findings indicate that both the semi-axe and fully-axe designs significantly reduced resistance compared with the traditional no-axe bow, with the semi-axe design achieving an average reduction of 9.17% and the fully-axe configuration reducing

resistance by 7.64%. Notably, the semi-axe bow outperformed the fully-axe design by an additional 1.42% in terms of resistance reduction.

This study challenges the prevailing belief that fully-axe bows provide optimal hydrodynamic performance, suggesting that semi-axe designs may offer superior resistance reduction. This insight has important implications for naval architecture and ship designs. Furthermore, this study underscores the effectiveness of CFD in optimizing ship designs, allowing for detailed fluid dynamics analysis without extensive physical testing. It also highlights the intricate relationship between the bow design, block coefficient, and resistance components, offering valuable insights into the factors influencing ship performance.

In terms of resistance and block coefficient correlation, the semi-axe bow hull demonstrated a drag reduction of up to 11.18% compared to the no-axe bow, whereas the fully-axe bow hull showed a decrease of up to 10%. The semi-axe bow's lower block coefficient contributed to an average 8% reduction in the resistance. The study also examined the resistance components, revealing that the wave resistance increased non-linearly with speed, particularly at higher velocities, with the fully-axe bow exhibiting the lowest wave resistance at approximately 2.4 m/s. The semi-axe bow achieved an average wave resistance reduction of 11 - 12%, whereas the fully-axe bow showed a reduction of 13 - 14% across all tested speeds. Additionally, the bow shape significantly influenced the fluid interaction with the hull, with the axe bow designs generating fewer waves in the forward region than the no-axe bow, which produced more waves. The semi-axe and fully-axe modifications resulted in lower wave-making resistance than the no-axe bow, further supporting the advantages of alternative bow designs in enhancing the efficiency of naval vessels.

ACKNOWLEGMENT

Authors thank LPPM-Universitas Hang Tuah for providing internal research funding under Contract Number B/004/UHT.C.2/II/2022. This study was supported by the Design Laboratory of the Universitas Hang Tuah.

CONFLICT OF INTEREST

Authors declare no potential conflicts of interest regarding the research, authorship, or publication of this article.

REFERENCES

Ahmad Fitriadhy, Rizuan Razali, Atiqah Yaakup, Utina, M.R., Abu Bakar, A., Kurniawan, A. and Ontowirjo, B., 2023. Computational investigation into predicting total resistance of axe-bow ships in calm water. CFD Letters, 15(11), pp.1–15. Available at: https://doi.org/10.37934/cfdl.15.11.115

Anderson, J.D., 1995. Computational fluid dynamics: The basics with applications. McGraw-Hill. Available at: https://books.google.co.id/books?id=phG_QgAACAAJ

ANSYS, Inc., 2020. ANSYS CFX-solver theory guide. Ansys Inc.

Bouckaert, B., 2012. Damen shipyard's first full axe-bow patrol vessel delivered to Cape Verdean coast guard. Offshore Energy. Available at: https://www.offshore-energy.biz/damen-shipyards-first-full-axe-bow-patrol-vessel-delivered-to-cape-verdean-coast-guard/

Butcher, J.G. and Elson, R.E., 2017. How did Indonesia become an archipelagic state? Available at: https://www.aspistrategist.org.au/indonesia-became-archipelagic-state/

Cribb, R. and Ford, M., 2009. Indonesia as an archipelago: Managing islands, managing the seas. In: R. Cribb and M. Ford (eds.) Indonesia beyond the water's edge: Managing an archipelagic state. ISEAS–Yusof Ishak Institute, pp.1–27. Available at: https://www.cambridge.org/core/product/5EA31A8D8BDA505938E29A9DE72104A6

Darmawan, A.R., 2022. Sovereignty, security and prosperity: Indonesia and the UN convention on the law of the sea. Available at: https://fulcrum.sg/sovereignty-security-and-prosperity-indonesia-and-the-un-convention-on-the-law-of-the-sea/

Djunarsjah, E. and Putra, A.P., 2021. The concept of an archipelagic province in Indonesia. IOP Conference Series: Earth and Environmental Science, 777(1), 012040. Available at: https://doi.org/10.1088/1755-1315/777/1/012040

Febrica, S., 2017. Maritime security and Indonesia: Cooperation, interests and strategies. Routledge.

ITTC, 2017. ITTC-recommended procedures and guidelines: Uncertainty analysis in CFD verification and validation methodology and procedures.

Keuning, J.A., Pinkster, J. and van Walree, F., 2018. Further investigation into the hydrodynamic performance of the AXE bow concept.

Keuning, J.A., van Terwisga, P.F. and Nienhuis, B., 2015. The possible application of an AXE bow on a 5000 ton frigate. Available at: https://doi.org/10.5957/FAST-2015-021

Kiryanto, Chrismianto, D., Hadi, E.S. and Firdhaus, A., 2021. Study of the effect on the addition of anti-slamming bulbous bow to total resistance in tugging supply vessel using CFD. IOP Conference Series: Earth and Environmental Science, 698(1), 012007. Available at: https://doi.org/10.1088/1755-1315/698/1/012007

Krank, B., 2019. Wall modeling via function enrichment for computational fluid dynamics. Technical University of Munich.

Kusuma, C., Ariana, I.M. and Ali, B., 2020. Redesign KCR 60m bow with axe bow type to reduce ship resistance. IOP Conference Series: Earth and Environmental Science, 557(1), 012033. Available at: https://doi.org/10.1088/1755-1315/557/1/012033

Lau, J.M., 2024. Indonesia's security relationship with the European Union: Prospects and possibilities for growth. In: The European Union as a security actor in the Indo-Pacific. Springer Nature Singapore, pp.115–130. Available at: https://doi.org/10.1007/978-981-97-4453-4_9

Liu, Z., Liu, W., Chen, Q., Luo, F. and Zhai, S., 2020. Resistance reduction technology research of high speed ships based on a new type of bow appendage. Ocean Engineering, 206, 107246. Available at: https://doi.org/10.1016/j.oceaneng.2020.107246

Menter, F.R., 1993. Zonal two equation κ-ω turbulence models for aerodynamic flows. AIAA Conference Proceedings, pp.1–21.

Menter, F.R., 1994. Two-equation eddy-viscosity turbulence models for engineering applications. AIAA Journal, 32(8), pp.1598–1605. Available at: https://doi.org/10.2514/3.12149

Menter, F.R., Kuntz, M. and Langtry, R., 2003. Ten years of industrial experience with the SST turbulence model. Proceedings of the 4th International Symposium on Turbulence, Heat and Mass Transfer, pp.625–632

Nasirudin, A., Sutiyo, S., Hudson, D. and Utama, I.K.A.P., 2025. Numerical investigation of trim and sinkage effect on resistance of a semi-planing monohull. CFD Letters, 17(1), pp.46–59. Available at: https://doi.org/10.37934/CFDL.17.1.4659

Priestnall, G., 1997. The regimes of archipelagic sea lanes passage and straits' transit passage: Similarities and differences. Maritime Studies, 96, pp.1–12. Available at: https://doi.org/10.1080/07266472.1997.10878494

Rijkens, A. and Mikelic, A., 2022. The hydrodynamic comparison between a conventional and an axe bow frigate hull. Proceedings of INEC 2022. Available at: https://doi.org/10.24868/10651

Sahri, A., Mustika, P.L.K., Dewanto, H.Y. and Murk, A.J., 2020. A critical review of marine mammal governance and protection in Indonesia. Marine Policy, 117, 103893. Available at: https://doi.org/10.1016/j.marpol.2020.103893

Samuel, S. et al., 2023. Analyzing the influence of water depth on total resistance in Ulstein X-bow configuration: A numerical study. E3S Web of Conferences, 465, 01020. Available at: https://doi.org/10.1051/e3sconf/202346501020

Samuel, S. et al., 2023. Investigation of an inverted bow on frigate hull resistance. Journal of Applied Fluid Mechanics, 17(1), pp.136–147. Available at: https://doi.org/10.47176/jafm.17.1.2122

Sandee, H., 2016. Improving connectivity in Indonesia: The challenges of better infrastructure, better regulations, and better coordination. Asian Economic Policy Review, 11(2), pp.222–238. Available at: https://doi.org/10.1111/aepr.12138

Suardi, S., Hidayat, T., Firmansyah, M.B. and Kyaw, A.Y., 2023. Impact of axe bow hull shape on patrol ship resistance, freeboard, and trim. Maritime Park Journal of Maritime Technology and Society, pp.16–21. Available at: https://doi.org/10.62012/mp.v2i1.25478

Utama, I.K.A.P., Sutiyo and Suastika, I.K., 2021. Experimental and numerical investigation into the effect of the axe-bow on the drag reduction of a trimaran configuration. International Journal of Technology, 12(3), pp.527–538. Available at: https://doi.org/10.14716/ijtech.v12i3.4659